Sigma J Eng Nat Sci, Vol. 43, No. 2, pp. 626–634, April, 2025

Sigma Journal of Engineering and Natural Sciences
Web page info: https://sigma.yildiz.edu.tr
DOI: 10.14744/sigma.2025.00049

Research Article

Design and development of carbon quantum dot-assisted fiber optic UV-A sensor

Sandra FRANCIS[1,4], Shashwati WANKAR[1], Utkarsh ALSET[1], Vivek CHAVAN[2], Suparna SODAYE[3], Sonawane CHANDRAKANT[1,4], Anand PANDEY[4], Abhinav KUMAR[6], Atul KULKARNI[1], Naveen Kumar GUPTA[7], Hitesh PANCHAL[5,*], Yogesh JADHAV[1,*]

[1]*Symbiosis Centre for Nanoscience and Nanotechnology, Symbiosis International Deemed University, Maharashtra, 412115, India*
[2]*Department of Physics, Sungkyunkwan University, Suwon, 16419, Republic of Korea*
[3]*Bhabha Atomic Research Centre, Trombay, Mumbai, 400085, India*
[4]*Symbiosis Institute of Technology, Symbiosis International Deemed University, Maharashtra 411043, India*
[5]*Department of Mechanical Engineering, Government Engineering College, Gujarat, 396001, India*
[6]*Department of Nuclear and Renewable Energy, Ural Federal University, Ekaterinburg, 620002, Russia*
[7]*Harcourt Butler Technical University, Uttar Pradesh, 208002, India*

ARTICLE INFO

Article history
Received: 08 October 2023
Revised: 25 November 2023
Accepted: 01 January 2024

Keywords:
Carbon Quantum Dots; Fiber-optic; Optical Sensor; Poly methyl methacrylate; Poly-vinyl alcohol; Ultraviolet-A radiation

ABSTRACT

Nanotechnology has opened up various health, environmental and sustainable energy possibilities, such as monitoring, remediation, and reducing global warming. In recent times, nanomaterials have elevated the conventional sensors to be more accurate, sensitive, and selective for detecting the desired analyte. Using carbon quantum dots (CQDs) it is possible to create fiber optic-based sensors that monitor ultraviolet-A (UV-A) radiation. Special tunable optoelectronic properties make CQDs a desirable option for sensing applications. This paper reports the development of a CQDs-based UV-A sensor based on fiber optics (FS-UV-A). The CQDs were prepared using citric acid and L-cysteine, and were characterized using UV-Visible spectroscopy and high resolution HRTEM. The synthesized CQDs possess high excitation and emission rates at 365 nm and 424 nm, respectively, which are ideal for UV-A sensing applications. A Cost effective FS-UV-A sensor was developed by utilizing the CQDs embedded in biodegradable poly-vinyl alcohol (PVA) polymer matrix coated on optical fiber. The use of optical fiber creates a smaller foot- print in turn making it portable and easy to use. With a detection limit of 0.2 μW/cm^2, the sensitivity and selectivity of the FS-UV-A towards UV-A radiation in the range of 0 – 1000 μW/cm^2 were evaluated. In addition, the sensor's 122 ms response time qualifies it for real-time use. It also showed good stability, which makes it a useful tool for measuring UV-A radiation in a variety of environmental conditions.

Cite this article as: Francis S, Wankar S, Alset U, Chavan V, Sodaye S, Chandrakant S, Pandey A, Kumar A, Kulkarni A, Gupta NK, Panchal H, Jadhav Y. Design and development of carbon quantum dot-assisted fiber optic UV-A sensor. Sigma J Eng Nat Sci 2025;43(2):626–634.

***Corresponding author.**
*E-mail address: engineerhitesh2000@gmail.com, nano4yash@gmail.com

This paper was recommended for publication in revised form by Editor-in-Chief Ahmet Selim Dalkilic

Published by Yıldız Technical University Press, İstanbul, Turkey

INTRODUCTION

Measurements of radiation exposure and UV detection are critical in various fields of human endeavor to detect and understand the effect of radiation on human body. The bands that make up the ultraviolet spectral region are often categorized according to their wavelength into three regions: UV-A, UV-B, and UV-C. The A-region (λ ¼ 315 nm to 400 nm) is where the atmosphere absorbs radiation the least [1]. The controlled exposure to UV is advantageous to some extent as it helps in absorption of certain vitamins such as vitamin D whereas, increased exposure to UV spectrum can lead to a variety of health problems, including macular degeneration, cataracts, corneal damage, skin discoloration, and worsened wrinkles. The basic concept of optical fiber-based sensing is widely recognized and shares many similarities with fiber communications i.e. the method of transmitting information sending pulses of infrared or visible light through an optical fiber.

The market parameters differ from the communications industry, and the implementation technology is also very different. The unique features of fiber-optic technology are its immunity to electromagnetic interference and physical damage and long-distance sensing capabilities. Moreover, fiber optic sensors with nanomaterial, such as carbon nanotubes, carbon quantum dots and graphene, have also been used to enhance the sensitivity of fiber optic sensors for the detection of UV-A light [2]. Carbon-nanostructures, particularly nanoscale CQDs, have been found to be an excellent material for various applications like bio-imaging, drug delivery [3-4], sensing [5-6], energy storage, and luminescent conversion due to their tunable optoelectronic properties [7]. These materials offer several advantages compared to traditional semiconductor quantum dots (QDs) and organic dyes. They exhibit high stability and solubility, remain chemically inert, and resist photo-bleaching thanks to their fluorophores [8-9]. Consequently, they find applications across various fields, such as solar cells [10-12], organic LEDs [13], photodetectors [14-15] photo catalysts, and super capacitors. These materials, known as CQDs, are nanoparticles with a carbon core and a functionalized or passivated surface, each measuring less than 10 nm. In the realm of optoelectronic sensors, quantum dots with higher quantum yield (QY) and material stability are highly desirable. Precise control over the position of the fluorescence band on the spectrum and its quantum yield is achievable by manipulating synthesis parameters. However, the scarcity of published works that compare the optical properties of these CQDs underscores the necessity for further research in this domain. Additionally, in the realm of UV-A radiation detection, different polymer membranes have been employed in the development of fiber optic sensors [16].

The ability of these membranes to absorb UV-A light makes it possible to detect UV-A radiation. There have been significant advancements in the use of fiber-optic technology as a sensor for UV-A radiation detection. This is primarily due to its immunity to electromagnetic interference, chemical and physical damage resistance, and ability to sense over long distances. This technology holds the potential to enhance the understanding of the effects of UV-A light and develop strategies to mitigate any adverse impacts [17]. Furthermore, the sensor system's small size makes it simple to utilize in portable and miniaturized applications, especially in minimally invasive medical procedures. This technology provides answers to a wide range of challenging instrumentation requirements in the biomedical field.

The potential to use a polymer membrane embedded with CQDs to create a UV-A spectrum sensor is the motivation behind this research. The research aims to investigate the factors influencing the effectiveness of fiber optic sensor technology in detecting and measuring UV-A radiation. To achieve this, development of a unique sensing device by synthesizing a flexible and transparent poly (vinyl alcohol) (PVA) polymer membrane with embedded CQDs could be achieved. This membrane was then coated onto a PMMA-based fiber optic. PMMA (Polymethyl methacrylate) is an easy to use material that can be used in any form for the detection of ultraviolet radiation. PVA was selected as the quantum dot embedding matrix because of its exceptional transparency and flexibility. It also makes quantum dot loading easier and strengthens the otherwise fragile PMMA fiber optic cable. Ensuring the high performance of CQDs in the fabrication of the UV-A sensor required careful optimization of the synthesis process. The stability, robustness, and accuracy of the developed UV-A radiation detection system was then evaluated.

MATERIALS AND METHODS

Materials

In this study, all chemicals were used as received without further purification except those specifically noted. Milli-Q water was used throughout the experiment. The citric acid (CA), L-Cysteine (L-Cyst), ethanol, and methylene chloride solvent were purchased from Sigma-Aldrich and Honeywell. The PVA was procured from Loba Chemie Pvt. Ltd. Standard PMMA optical fiber AWM 5310 80 C VW-1 GHCP-4001-U, Mitsubishi rayon co ltd was used. Before use, all glassware was cleaned with a dilute acid solution, rinsed with distilled water, and oven-dried.

Carbon Quantum Dots (CQDs) Synthesis

The synthesis of CQDs has been performed using the reported procedure [18-20] with minor modifications. In a typical synthesis of CQDs, a mixture of 10mM of CA and 4mM of L-Cys (1:0.4) was used. The (CA + L-Cys) white powdered precursors were homogeneously mixed within the borosilicate glass vial, followed by oven irradiation for 2 min. Initially, the powder in a white hue transformed into a grey-black shade through the process of microwave

pyrolysis. The resultant was then ground into a fine powder using a mortar pestle. A stock solution of CQDs (5 mg/ml) was prepared by combining the obtained powder with milli-Q and filtering it using a glass syringe. The obtained product is filtered and stored at 4 degree in milli Q water for characterization of the materials and further application.

CQDS Coating On Fiber Optic

The fabrication process of the PVA-CQD composite, as shown in Fig. 1 (a), began by dissolving 2 grams of PVA in 20 mL of Milli -Q water in a beaker. This dissolution process was carried out under constant agitation utilizing heat at a temperature of 100 °C in order to achieve a thick homogenous blend solution [20-21]. Once a homogenous solution of PVA was obtained, 0.1 mg/ml of CQDs from the prepared stock solution was added to the PVA blend while maintaining constant stirring. The solution was uniformly coated on the spliced fiber optic segment using a dip-coating unit set at 45 °C infra-red dry (IR-D) chamber. The coated fiber optic segment is exposed under 365 nm UV-A radiation. The response was measured using a spectrophotometer Ocean Optics FLAME T-XR1-ES for further signal acquisition and interpretation.

FS-UV-A Sensor Fabrication

The PMMA-based single-mode fiber-optic (SMFO), as shown in Fig. 1 having a 980 µm core, 20 µm cladding layer, and an overall diameter with a protective jacket of 2.2 µm was selected based on previous studies [22-26]. Dimensions of the fiber are pre-defined. The fiber-optic protective cover of 10 mm was mechanically removed using a surgical blade of a corslet high-precision fiber-optic cleaver cutter [27] from one end of the 1 m long fiber-optic long segment. The cladding of 20 µm was removed to achieve a bare polymer core by applying a special setting [27], taking care that the surface of the fiber-optic polymer core was not scratched or damaged in any way. The spliced area was further treated with acetone, washed with a large quantity of water, and dried in an IR chamber. The fabricated fiber optic was then dipped into the prepared CQDs blend at an optimized rate of 2 m/s (drying time, T dry = 10 s and dipping time, T dip = 2 s) with a total of 250 dips per fiber optic segment using a dip-coating unit (Holmarc, HO-TH-02B). Ten such fiber optic segments were prepared and designated fiber optic sensor-based UV-A (FS-UV-A) which was used further for sensor functionality, data reproducibility, and repeatability.

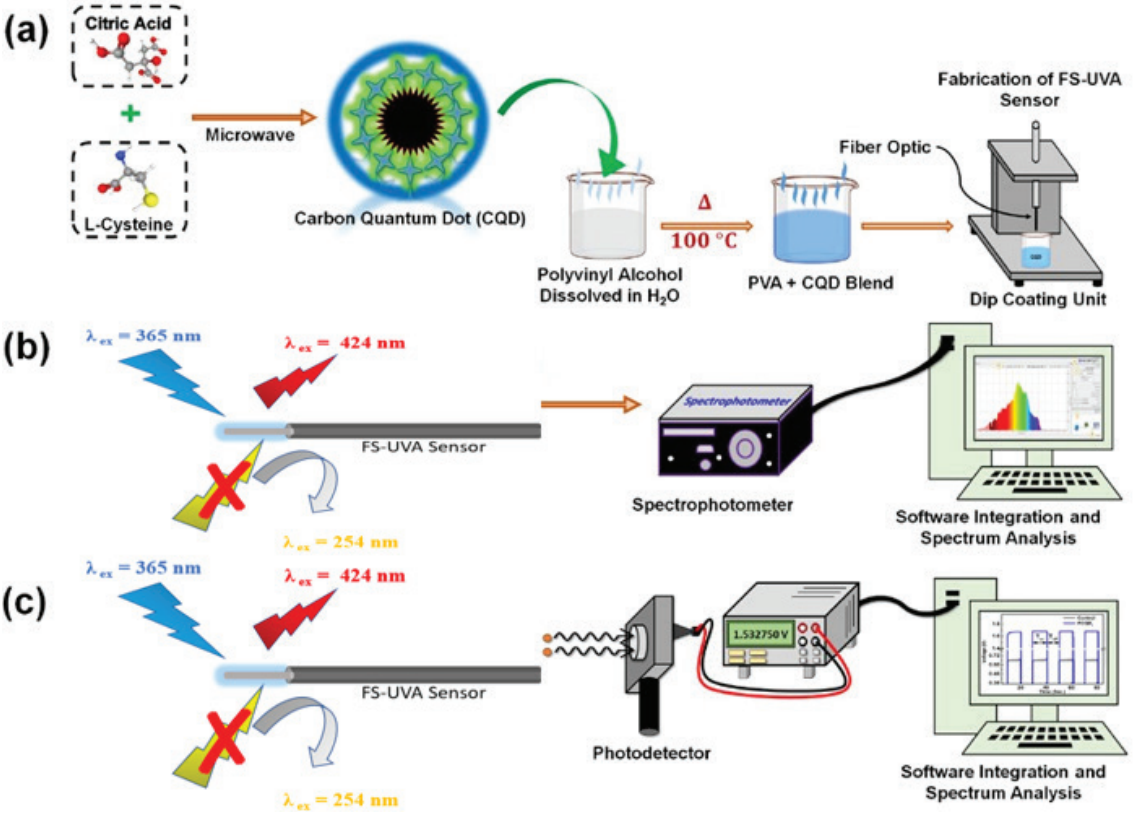

Figure 1. The schematic illustration shows (a) the synthesis of CQDs, followed by making a blend of PVA dissolved in H_2O at 100 °C and adding CQDs from the stock solution into the PVA blend. Subsequent coating of the PVA a blend on the fiber optic segment using a dip coating unit, (b) the responses of the fabricated fiber optic segment under excitation of 365 nm UV-A radiation shows emission at 424 nm and 254 nm UV-B radiation no emission and further connected to the spectrophotometer for the signal acquisition and interpretation.

Materials and Sensor Characterization

Optical properties of the synthesized water dispersed CQDs were studied using a Jasco V-750 UV-visible spectrophotometer. Further, the size, morphology and particle size distribution were studied by High Resolution Transmission Electron Microscopy (HR-TEM) using a FEI Tecnai G2, F30 TEM system. ImageJ software version 1.46r was used to determine the particle size distribution histogram from HR-TEM micrographs. The response was measured on a miniature spectrophotometer ocean optics FLAME T-XR1-ES for further signal acquisition and interpretation. Additionally, a digital multimeter (Keithley, DMM6500) was employed for data acquisition and evaluation of the FS-UV-A sensor [28].

Measurement Setup System

All the experiments were performed in a dark room to minimize the effect and interference of ambient light and complete occlusion to outside light on the optical experiments. Figure 1 (a) is the schematic illustration showing the synthesis of CQDs later dissolved in PVA and then dip coated. Figure 1 (b) shows the optical fiber connected to the miniature spectrophotometer (Ocean Optics, FLAME). Figure 1 (c) shows one end of the fiber-optic connected to the photodetector (THORLABS, PDA36A2) for the FS-UV-A sensor preparation, as shown in Figure 1 (c). A source of UV-A light (365 nm) was directed towards the opposite end of the fiber-optic segment [29]. In addition, each fabricated FS-UV-A segment's voltage responses from the photodetector were recorded for data analysis.

RESULTS AND DISCUSSION

Structural Studies

The morphology and structure of the synthesized CQDs were investigated using high-resolution transmission electron microscopy (HRTEM), as shown in Figure 2 (a). The HRTEM analysis demonstrates that the CQDs exhibit uniform particle distribution with an average particle size of 3 ± 0.75 nm. The lattice spacing of the CQDs, as shown in Figure 2(an inset), was measured to be 2.207 Å, consistent with the (100) plane spacing of sp2 carbon [30-32]. The particle size distribution of the CQDs, as shown in Figure 2(b), ranged between of 3 ± 0.75 with a maximum uniform distribution. This indicates that the small size and spherical shape distribution of the CQDs obtained were consistent and within an acceptable range.

Figure 2 (c) illustrates the absorption spectrum of CQDs dispersed in water, showing a prominent band with a peak (λmax) at 342 nm. Within the 250 – 300 nm wavelength

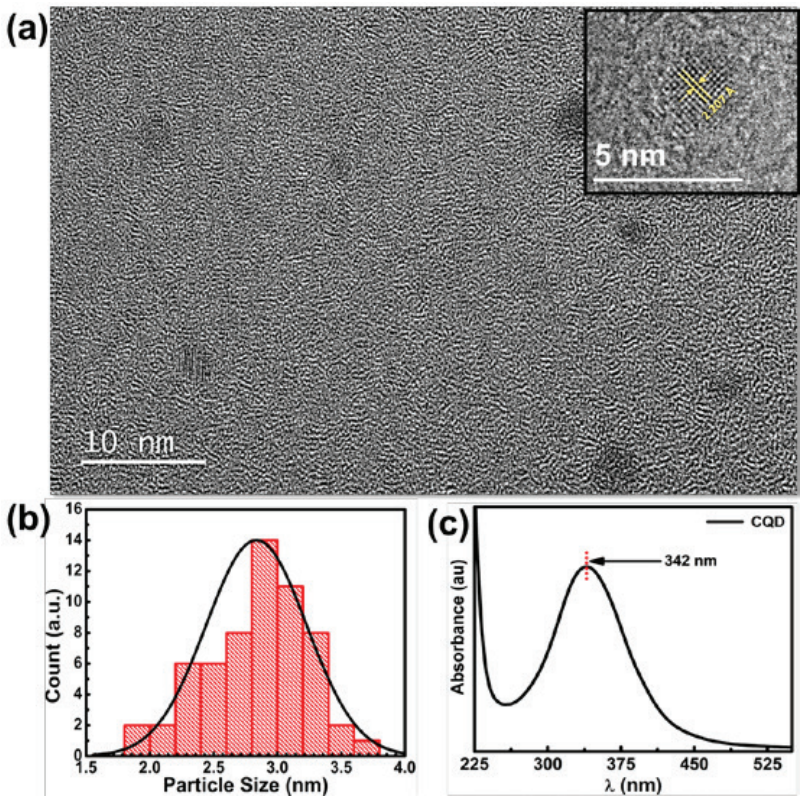

Figure 2. (a) TEM and HRTEM images of synthesized CQDs, low resolution at 10 nm, and the high resolution of CQD at 5 nm crystalline lattices can be seen, (b) shows the size distribution of CQDs corresponding to the TEM, and (c) CQDs absorbance spectra at 342 nm.

range, the absorption is attributed to the ($\pi\pi - \pi\pi*$) conjugated carbon bonds of CQDs, while the longer-wavelength peak results from ($nn - \pi\pi*$) transitions in the "C = O" bonds of CQDs. The absorption on the longer-wavelength side (λ > 400 nm) can be linked to the presence of surface functional groups, such as –SH and C – N, N – H bonds [16].

It is important to note that the shape profile of the fluorescence excitation spectrum differs from the absorption spectrum of the CQDs. With an increase in the excitation wavelength from 250 – 350 nm, the fluorescence intensity of the CQDs is seen to increase considerably. Due to this exposure, physicochemical properties change due to the size of CQDs, which is inversely proportional to the energy level present in the band gap and therefore alters the frequency of light emitting distinct fluorescence [1]. Moreover, the variation in peak features may be attributed to the absorption of the "C –" component of CQDs and the contribution of the "C = O" groups, which have relatively weak absorption characteristics. These groups emit fluorescence simultaneously, which is evident in the excitation spectra. As the excitation wavelength increases from 250 – 350 nm, the fluorescence intensity of the CQDs significantly rises. Consequently, the peak of the fluorescence spectrum shifts towards longer wavelengths, specifically at 424 nm when exposed to specific 365 nm light radiation.

Figure 3 (a) displays the emission spectra at 424 nm. From figure 3(a), the peak-to-peak intensity variation was observed by changing the distance from 1mm to 75mm between CQDs based optical fibre sensor and 365nm LED M365F1. The control sample response is represented as a reference which illustrates the highest intensity at 1mm distance at a maximum current of 700 mA, 3080 mW of the LED light source. To compare the luminescent properties of CQDs when exposed to 365 nm and increased the distance between the 365 nm light sources from 1 mm to 75 mm on the FS-UV-A. From figure 3(b), it is evident that with respect to change in time the amplitude of the voltage changes. At a peak current of 700 mA at 365 nm LED M365F1, the peak voltage obtained at the output of the photodetector measured using DMM6500 for CQD is 1.6477 V. The change obtained between the peak amplitude of control and CQDs is 0.86 V. As depicted in Figure 3 (a, b) the CQDs efficiently absorb the incident 365 nm light in the UV-A range. This results in more excitation observed at 365 nm, leading to emission at 424 nm. Consequently, the primary contributor to the overall luminescence in the synthesized CQDs is the presence of S- and N-groups incorporated into the CQDs. Consequently, the fabricated FS-UV-A sensor is further employed for quantifying voltage pulses.

Figure 4(a) illustrates the T_r and T_d of the CQDs to delve into the voltage amplitude analysis. The sensor exhibits sensitivity during the T_d-region, transitioning from a higher to lower amplitude state, ranging from 1.66 V to 0 V, resembling the characteristics of an LED photodiode. Therefore, the shift in peak wavelength, representing the change in voltage of the reflected light, can be monitored simultaneously using the proposed FS- UV-A sensor. Figure 4(b) initially shows T_{on}/T_{off} with T_{on} = 10 min and T_{off} = 10 sec, then with T_{on} at 20 min and T_{off} at 20 sec. By analyzing Figure 3 and Figure 4(b), calculation of output energy and instantaneous peak power between the control sample can be done and mathematical correlation between control sample and CQDs can be calculated. In a continuous wave laser, there are small fluctuations, but basically the minimum, average and maximum power of a continuous wave laser are the same. In a pulsed one, small burst of energy is separated by down times where no light is emitted. So the minimum power is usually 0 W and the maximum power is at peak when the intensity reaches its maximum value. For calculation of peak power of a laser beam, divide the energy in each pulse by the duration of the pulse that is known as pulse width. Calculation of peak power density is done by dividing the peak power by the area of the beam's cross-section at a given distance.

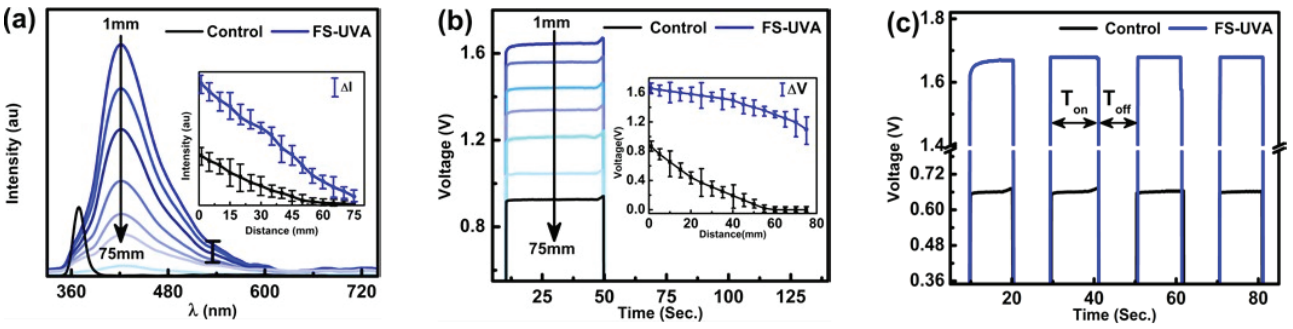

Figure 3. (a) Comparison of intensity between FS-UV-A and control sample is recorded by varying the distance of the 365 nm light source from 1 mm to 75 mm. (b) Illustrates change in voltage with respect to distance for both control and CQDs, exhibiting superior UV-A sensing. The inset illustrates the intensity and voltage drop-down beyond the distance of 55 mm. (c) T_{on} / T_{off} pulses of the voltage vs time response recorded between the control and CQDs coated on the fiber-optic core.

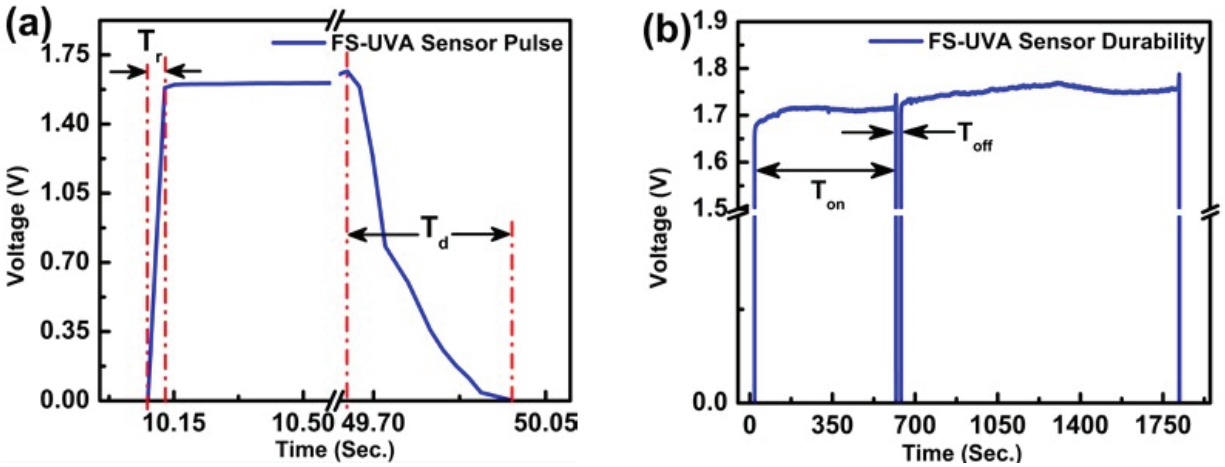

Figure 4. (a) The sensitivity of the UV-A sensor is illustrated based on the rise time, T_r= 122 ms. and the decay time, T_d = 603 ms, respectively. (b) The stability test is performed for 30 min on the developed sensitive fiber optic UV-A sensor, demonstrating excellent reliability and stability over the period.

Knowing the average power of the laser, the energy per pulse by dividing it by the f repetition rate can be found out.

$$Peak\ power\ density\left(\frac{W}{cm^2}\right)=\frac{Energy\ per\ pulse\ (J)}{Pulse\ width(s)\times Beam\ area\ (cm^2)} \quad (1')$$

Hence, from 1' we get 2',

$$Peak\ power\ density\left(\frac{W}{cm^2}\right)\frac{Average\ power(W)}{Repetition\ rate\ (Hz)\times Pulse\ width(s)\times Beam\ area\ (cm^2)} \quad (2')$$

Considering the total period (Dt) = 1/f repetition (in sec.) for the control and CQD sample (from Figure 3 & 4(b)), the E pulse is calculated by specifying the maximum peak-pulse power (P peak-pulse) for the control(from 2'),

$$E_{pulse}=\frac{P_{average}}{f_{repetition}}=\frac{3080\ mW}{4.4\ mHz}=\ 7\ mJ \quad (1)$$

The energy per peak pulse voltage is very low (here, 7 mJ); however, the peak-pulse power can be calculated as (from 2'),

$$P_{peak-pulse}=\frac{P_{average}}{f_{repetition}\times t}=\frac{3080\ m\ W}{4.4\ mHz\times 10\ fs}=700\ \text{mW} \quad (2)$$

Where,

E_{pulse}= measurement of the total emission of one pulse during Ton time only;

$P_{average}$= average power of the optical uniform pulse over the period Δt; and

$P_{peak\text{-}pulse}$= instantaneous maximum peak-pulse power output

From eq. (1) and (2), the total $P_{peak\text{-}pulse}$ = 700 mW for the control sample at 0.8665 V. Similarly, at 1.66 V, the total $P_{peak\text{-}pulse}$ = 1341.02 mW. The difference in peak power output between the control and CQDs samples is 641.02 mW. Therefore, the efficiency of the sensor between the control and CQDs sample is,

$$P_{peak-pulse}=\frac{(P_{peak-pulse\ of\ PCQD_1})-(P_{peak-pulse\ of\ Control})}{P_{peak-pulse\ of\ Control}}=91.57\ \%$$

Furthermore, from Figure 3(b), the developed sensitive fiber optic UV-A sensor demonstrates exceptional stability for a total runtime duration of 1800 s (30 min).

A manual on/off switching method at every 10 s. was performed to test the temporal response of the developed sensor (as shown in Figure 4(b)). It was observed that even

Table 1. Comparison table with the reported work

Sr no.	Sensor	Analyte	Sensor response time	Reference
1.	ZnO QD-based photodetector	Deep UV	85 ms	33
2.	Photochromic dye-doped optical microfiber	UV light	~10000 ms	34
3.	Ag-decorated ZnO micro-pillar Fiber sensor	All-UV	0.04 ms	35
4.	Optical microfiber sensor	UV light	~10000 ms	36
5.	p-CuZnS/n-TiO2 UV photodetector (PD)	UV light	< 200 ms	37
6.	Azobenzene-polymer-capped Optical-fiber	UV light	200 ms	38
7.	CQD based FS-UV-A sensor	UV-A radiation	122 ms	This work

if there is a significant insertion loss, the sensor response can still be distinguished from the photodetectors' noise signal. In Figure 3 (c), the periodic response of the FS-UV-A is observed comparing the control sample, which is PMMA coated with non-loaded PVA. From Figure 4 (a, b) the output energy and instantaneous peak power can be calculated between the control FS-UV-A and co-relate mathematically with fabricated FS-UV-A. Considering the total period (Δt) for the control and FS-UV-A, the 7 mJ of E_{pulse} is calculated by specifying the maximum peak-pulse power ($P_{peak-pulse}$) for the control. The energy per peak pulse voltage is very low (here, 7 mJ); however, the peak-pulse power is calculated as 700 mW for the control FS-UV-A at 0.8665 V. Similarly, at 1.66 V, the total Ppeak–pulse is 1341.02 mW. The difference in peak power output between the control and FS-UV-A is 641.02 mW. Thus, the efficiency, meaning the output voltage response to the input UV-A light of the FS-UV-A sensor, constitutes 91.57%, indicating the potential of CQDs for developing environmentally sustainable optoelectronic devices. Future nanotechnology research could explore CQDs' possibilities in developing sustainable and cost-effective optoelectronic devices. Table 1 shows the previous reported work compared with current result.

CONCLUSION

Successful synthesis of CQDs by low-cost microwave techniques was achieved. The fabricated FS-UV-A showed an excellent response to the UV –A radiation at 365 nm. The study examined the morphology and structure of CQDs using high-resolution transmission electron microscopy. The results of the analysis indicated that the CQDs had an average particle size of 3 ± 0.75 nm and good uniformity and particle size distribution. UV-A radiation detection using CQDs in a fiber-optic sensor system has produced encouraging results. CQDs showed a band in their absorption spectrum that peaked at 342 nm. When their excitation wavelength was changed from 250 to 350 nm, they showed an increase in fluorescence intensity, with emission occurring at 424 nm. The synthesized CQDs were then utilized to create an FS-UV-A sensor, which displayed an efficiency of 91.57% in peak-pulse power generation in response to the input UV-A light and a periodic response. Additionally, the sensor's 122 ms response time makes it appropriate for real-time measurement. This illustrated the wide range of potential applications for the CQDs-assisted FS-UV-A sensor system, where the functionalized optical fiber functions as a stand-alone application. The material that are used for preparation of the CQDs along with the polymers and the optical fiber used are all environment friendly and highly biodegradable. Using these materials for sensing applications is an indicator of a novel application. The use of optical fiber having smaller foot- print (design and size) and the modification of the optical fiber is in itself a novel method to create a sensor for UV sensing. The proposed methodology is simple, user-friendly, is analyte process free and the sensor is portable. Future research can be done considering the fact that this UV sensor can be used in print industry for solvent handling and dyeing processes. Similarly, future scope is seen in automotive industry, robotics and pharmaceutical industry.

ACKNOWLEDGEMENTS

The authors thank 'Symbiosis Centre for Nanoscience and Nanotechnology'(SCNN). Authors (UA and SF) thank Bhabha Atomic Research Centre (BARC) in Trombay, Maharashtra, India, under the Board of Research in Nuclear Sciences (BRNS) for the fellowship. The authors (AK and YJ) thank Symbiosis International University for their support.

COMPETING INTERESTS

This research project was funded by the Bhabha Atomic Research Centre (BARC) in Trombay, Maharashtra, India, under the Board of Research in Nuclear Sciences (BRNS) Project Sanction No. 58/14/16/2020-BRNS/37002. The project was conducted in collaboration with the Symbiosis Centre for Nanoscience and Nanotechnology (SCNN) at Symbiosis International (Deemed University) in Lavale, Pune.

AUTHOR CONTRIBUTIONS

Utkarsh Alset: Conceptualization, experimental design & study, data curation & interpretation, original draft writing. Sandra Francis: Data curation & interpretation, experimental design & study, original draft writing review of draft and editing. Shashwati Wankar: Set-up design, experimental study, draft writing, and editing. Vivek Chavan: Draft writing, and editing. Suparna Sodaye: resources, project administration, review of draft. Hitesh Panchal: Draft editing and reviewing. Abhinav Kumar: Data curation. Naveen Kumar Gupta: Supporting experiment. Chandrakant Sonawane: Data curation and draft editing. Anand Pandey: Data curation and draft editing. Atul Kulkarni: Conceptualization, resources, data validation, project administration, writing, review, and editing of the original draft. Yogesh Jadhav: Conceptualization, Experimental design and study, and data interpretation, editing of the original draft.

DATA AVAILABILITY STATEMENT

The authors confirm that the data that supports the findings of this study are available within the article. Raw data that support the finding of this study are available from the corresponding author, upon reasonable request.

ETHICS

There are no ethical issues with the publication of this manuscript.

REFERENCES

[1] Sutanto H, Alkian I, Romanda N, Lewa IWL, Marhaendrajaya I, Triadyaksa P. High green-emission carbon dots and its optical properties: Microwave power effect. AIP Adv 2020;10:055008.[CrossRef]

[2] Şen P, Hirel C, Andraud C, Aronica C, Bretonnière Y, Mohammed A, et al. Fluorescence and FTIR spectra analysis of *trans*-A_2B_2-substituted di- and tetra-phenyl porphyrins. Materials 2010;3:4446-4475. [CrossRef]

[3] Nuengmatcha P, Sricharoen P, Limchoowong N, Mahachai R, Chanthai S. The use of $S_2O_8^{2-}$ and H_2O_2 as novel specific masking agents for highly selective "turn-on" fluorescent switching recognition of CN^- and I^- based on Hg^{2+}–graphene quantum dots. RSC Adv 2018;8:1407–1417. [CrossRef]

[4] Wang D, Chen JF, Dai L. Recent advances in graphene quantum dots for fluorescence bioimaging from cells through tissues to animals. Part Part Syst Charact 2015;32:515–523. [CrossRef]

[5] Li K, Liu W, Ni Y, Li D, Lin D, Su Z, et al. Technical synthesis and biomedical applications of graphene quantum dots. J Mater Chem B 2017;5:4811–4826. [CrossRef]

[6] Xu Q, Zhou Q, Hua Z, Xue Q, Zhang C, Wang X, et al. Single-particle spectroscopic measurements of fluorescent graphene quantum dots. ACS Nano 2013;7:10654–10661. [CrossRef]

[7] Molaei MJ. Carbon quantum dots and their biomedical and therapeutic applications: A review. RSC Adv 2019;9:6460–6481. [CrossRef]

[8] Lim SY, Shen W, Gao Z. Carbon quantum dots and their applications. Chem Soc Rev 2015;44:362–381. [CrossRef]

[9] Zuo P, Lu X, Sun Z, Guo Y, He H. A review on syntheses, properties, characterization, and bioanalytical applications of fluorescent carbon dots. Microchim Acta 2016;183:519–542. [CrossRef]

[10] Tang Q, Zhu W, He B, Yang P. Rapid conversion from carbohydrates to large-scale carbon quantum dots for all-weather solar cells. ACS Nano 2017;11:1540–1547. [CrossRef]

[11] Ryu J, Lee JW, Yu H, Yun J, Lee K, Lee J, et al. Size effects of a graphene quantum dot modified-blocking TiO_2 layer for efficient planar perovskite solar cells. J Mater Chem A 2017;5:16834–16842. [CrossRef]

[12] Tsai ML, Wei WR, Tang L, Chang HC, Tai SH, Yang PK, et al. Si hybrid solar cells with 13% efficiency via concurrent improvement in optical and electrical properties by employing graphene quantum dots. ACS Nano 2016;10:815–821. [CrossRef]

[13] Song SH, Jang MH, Chung J, Jin SH, Kim BH, Hur SH, et al. Highly efficient light-emitting diode of graphene quantum dots fabricated from graphite intercalation compounds. Adv Opt Mater 2014;2:1016–1023. [CrossRef]

[14] Arvand M, Hemmati S. Analytical methodology for the electro-catalytic determination of estradiol and progesterone based on graphene quantum dots and poly(sulfosalicylic acid) co-modified electrode. Talanta 2017;174:243–255. [CrossRef]

[15] Niu Y, Wang J, Zhang J, Shi Z. Graphene quantum dots as a novel conductive additive to improve the capacitive performance for supercapacitors. J Electroanal Chem 2018;828:1–10. [CrossRef]

[16] Zhao R, He T. Estimation of 1-km resolution all-sky instantaneous erythemal UV-B with MODIS data based on a deep learning method. Remote Sens 2022;14:384. [CrossRef]

[17] Srivastava JK, Shankar E, Gupta S. Chamomile: A herbal medicine of the past with a bright future. Mol Med Rep 2010;3:895–901. [CrossRef]

[18] Lopez T, Ramillien G, Antoine R, Darrozes J, Cui YJ, Kerr Y. Investigation of short-term evolution of soil characteristics over the Lake Chad basin using GRACE data. Remote Sens 2018;10:924. [CrossRef]

[19] Jiang K, Sun S, Zhang L, Lu Y, Wu A, Cai C, et al. Red, green, and blue luminescence by carbon dots: Full-color emission tuning and multicolor cellular imaging. Angew Chem 2015;127:5450–5453. [CrossRef]

[20] El-Shamy AG, Zayied HSS. New polyvinyl alcohol/carbon quantum dots (PVA/CQDs) nanocomposite films: Structural, optical, and catalysis properties. Synth Met 2020;259:116218. [CrossRef]

[21] Xu L, Zhang Y, Pan H, Xu N, Mei C, Mao H, et al. Preparation and performance of radiata-pine-derived polyvinyl alcohol/carbon quantum dots fluorescent films. Materials 2019;13:67. [CrossRef]

[22] Zanon MC, Silva VN, Barbero AP, Ribeiro RM. Practical splicing of poly-methyl-methacrylate plastic optical fibers. Appl Opt 2018;57:812–816. [CrossRef]

[23] Kulkarni A, Lee JH, Nam JD, Kim T. Thin film-coated plastic optical fiber probe for aerosol chemical sensing applications. Sens Actuators B Chem 2010;150:154–159. [CrossRef]

[24] Kulkarni A, Na J, Kim YJ, Baik S, Kim T. An evaluation of the optical fiber beam as a force sensor. Opt Fiber Technol 2009;15:131–135. [CrossRef]

[25] Tagad CK, Dugasani SR, Aiyer R, Park S, Kulkarni A, Sabharwal S. Green synthesis of silver nanoparticles and their application for the development of optical fiber-based hydrogen peroxide sensor. Sens Actuators B Chem 2013;183:144–149. [CrossRef]

[26] Thorlabs. PDA36A2 Si Switchable gain detector user guide. Available at: https://physique.ens-lyon.fr/sites/default/files/materiel-physique-notices/N018-050.pdf. Accessed March 17, 2025.

[27] Keithley Instruments. Model DMM6500 6½-digit multimeter with scanning. Calibration and adjustment manual. 2022.

[28] Thorlabs. M365F1 – 365 nm, 3.0 mW (Min) fiber-coupled LED, 700 mA, SMA.

[29] Mitra S, Aravindh A, Das G, Pak Y, Ajia I, Loganathan K, et al. High-performance solar-blind flexible deep-UV photodetectors based on quantum dots synthesized by femtosecond-laser ablation. Nano Energy 2018;48:551–559. [CrossRef]

[30] Dong Y, Pang H, Yang HB, Guo C, Shao J, Chi Y, et al. Carbon-based dots co-doped with nitrogen and sulfur for high quantum yield and excitation-independent emission. Angew Chem Int Ed 2013;52:7800–7804. [CrossRef]

[31] Kalytchuk S, Poláková K, Wang Y, Froning JP, Cepe K, Rogach AL, et al. Carbon dot nanothermometry: Intracellular photoluminescence lifetime thermal sensing. ACS Nano 2017;11:1432–1442. [CrossRef]

[32] Lin H, Huang J, Ding L. Preparation of carbon dots with high-fluorescence quantum yield and their application in dopamine fluorescence probe and cellular imaging. J Nanomater 2019;2019:5037243. [CrossRef]

[33] Mitra S, Aravindh A, Das G, Pak Y, Ajia I, Loganathan K, et al. High-performance solar-blind flexible deep-UV photodetectors based on quantum dots synthesized by femtosecond-laser ablation. Nano Energy 2018;48:551–559. [CrossRef]

[34] Chen GY, Wang Z. Towards extremely sensitive ultraviolet-light sensors employing photochromic optical microfiber. J Sensors 2015;2015:586318. [CrossRef]

[35] Ma D, Wang Y, Chen C, Cai Z, Zhang J, Liao C, et al. Fast all-fiber ultraviolet photodetector based on an Ag-decorated ZnO micro-pillar. Opt Express 2023;31:5102–5112. [CrossRef]

[36] Chen GY, Lancaster DG, Monro TM. Optical microfiber technology for current, temperature, acceleration, acoustic, humidity, and ultraviolet light sensing. Sensors 2017;18:72. [CrossRef]

[37] Xu X, Chen J, Cai S, Long Z, Zhang Y, Su L, et al. A real-time wearable UV-radiation monitor based on a high-performance p-CuZnS/n-TiO_2 photodetector. Adv Mater 2018;30:1803165. [CrossRef]

[38] Cho HT, Seo GS, Lim OR, Shin W, Jang HJ, Ahn TJ. Ultraviolet light sensor based on an azobenzene-polymer-capped optical-fiber end. Curr Opt Photonics 2018;2:303–307.